

Spin reorientation of the Fe moments in $\text{Eu}_{0.5}\text{Ca}_{0.5}\text{Fe}_2\text{As}_2$: Evidence for a strong interplay of Eu and Fe magnetism

W. T. Jin,^{1,*} M. Meven,^{2,1} A. P. Sazonov,^{2,1} S. Demirdis,¹ Y. Su,¹ Y. Xiao,³ Z. Bukowski,⁴ S. Nandi,^{5,6} and Th. Brückel^{6,1}

¹Jülich Centre for Neutron Science JCNS at Heinz Maier-Leibnitz Zentrum (MLZ),
Forschungszentrum Jülich GmbH, Lichtenbergstraße 1, D-85747 Garching, Germany

²RWTH Aachen University, Institut für Kristallographie, D-52056 Aachen, Germany

³School of Advanced Materials, Peking University Shenzhen Graduate School, Shenzhen 518055, China

⁴Institute of Low Temperature and Structure Research, Polish Academy of Sciences, 50-422 Wrocław, Poland

⁵Department of Physics, Indian Institute of Technology, Kanpur 208016, India

⁶Jülich Centre for Neutron Science JCNS and Peter Grünberg Institut PGI,
JARA-FIT, Forschungszentrum Jülich GmbH, D-52425 Jülich, Germany

Using complementary polarized and unpolarized single-crystal neutron diffraction, we have investigated the temperature-dependent magnetic structures of $\text{Eu}_{0.5}\text{Ca}_{0.5}\text{Fe}_2\text{As}_2$. Upon 50 % dilution of the Eu sites with isovalent Ca^{2+} , the Eu sublattice is found to be still long-range ordered below $T_{\text{Eu}} = 10$ K, in the A-typed antiferromagnetic (AFM) structure. The moment size of Eu^{2+} spins is estimated to be as large as $6.74(4) \mu_B$ at 2.5 K. The Fe sublattice undergoes a spin-density-wave transition at $T_{\text{SDW}} = 192(2)$ K and displays an in-plane AFM structure above T_{Eu} . However, at 2.5 K, the Fe^{2+} moments are found to be ordered in a canted AFM structure with a canting angle of $14(4)^\circ$ out of the ab plane. The spin reorientation of Fe below the AFM ordering temperature of Eu provides a direct evidence of a strong interplay between the two magnetic sublattices in $\text{Eu}_{0.5}\text{Ca}_{0.5}\text{Fe}_2\text{As}_2$.

PACS numbers:

I. INTRODUCTION

The discovery of superconductivity (SC) with the critical temperature $T_c = 26$ K in fluorine-doped LaFeAsO in 2008 has opened up an “iron age of superconductivity”.¹ Shortly after that, T_c above 50 K was achieved in $R\text{FeAsO}_{1-x}\text{F}_x$ (“1111” system, $R = \text{Ce}, \text{Sm}, \text{Pr}, \text{Nd}, \text{and Gd}$) with R being a rare-earth element.^{2–5} SC with T_c up to 38 K was also realized by various chemical substitutions in the ternary “122” compounds $A\text{Fe}_2\text{As}_2$ with A being an alkaline-earth-metal element (Ca, Ba, Sr) or the rare-earth element Eu.^{6–8} It was well confirmed that the SC in the iron pnictides emerges upon the suppression of the static long-range spin-density-wave (SDW) order of Fe by means of chemical doping or applying external pressure.^{9,10} Although SC is compatible with the localized moments of the rare-earth ions in either “1111” or “122” system,^{11–14} how the magnetism of Fe and rare-earth element interact with each other is still not well elucidated.

In-depth experimental studies performed on quaternary “1111” $R\text{FeAsO}$ system have provided compelling evidences that there is a strong coupling of Fe and R magnetism for $R = \text{Ce}, \text{Sm}, \text{Pr}, \text{and Nd}$, respectively.^{15–19} However, for ternary EuFe_2As_2 compounds, it is quite controversial regarding the strength of the interplay of Fe and Eu magnetism.^{20–27} As a special member of the “122” system, EuFe_2As_2 has drawn tremendous attention, due to the strong spin-charge-lattice coupling and doping- or pressure-induced coexistence of SC and strong ferromagnetism.^{28–35} In a purely ionic picture, the S -state (orbital moment $L = 0$) Eu^{2+} rare-earth ion has a $4f^7$ electronic configuration and a total electron spin $S = 7/2$, corresponding to a theoretical total effective magnetic moment of $\mu_{\text{eff}} = g\sqrt{S(S+1)} = 7.94 \mu_B$ (with the Landé factor $g = 2$).³⁶ The non-superconducting parent compound EuFe_2As_2 undergoes a structural phase transition from a tetragonal to an

orthorhombic phase at 190 K, concomitant with a SDW ordering of the itinerant Fe moments. In addition, the localized Eu^{2+} spins order below 19 K in the A-type antiferromagnetic (AFM) structure (ferromagnetic layers stacked antiferromagnetically along the c axis).³⁷

According to previous neutron and non-resonant x-ray magnetic scattering experiments,^{20,21} the coupling between the Eu and Fe sublattices in EuFe_2As_2 was found to be negligible, which was further supported by density-functional electronic structure calculations.²² Also, a direct optical pump-probe showed a slow response of the Eu^{2+} spins to the optical excitation of the itinerant carriers on the FeAs layers, suggesting a weak coupling between the two sublattices.²³ In contrast, magnetic Compton scattering on $\text{EuFe}_2(\text{As}_{0.73}\text{P}_{0.27})_2$ indicated that the magnetism of Fe gets enhanced when the Eu magnetic order sets in.²⁴ In addition, nuclear magnetic resonance (NMR) and Mössbauer spectroscopy measurements revealed a strong coupling between the localized Eu^{2+} moments and the conduction d electrons on the FeAs layers in Co-doped EuFe_2As_2 .^{25,26} Recently, by performing x-ray resonant magnetic scattering (XRMS) measurement on underdoped $\text{Eu}(\text{Fe}_{0.94}\text{Ir}_{0.06})_2\text{As}_2$, we have observed the magnetic polarization of the Ir $5d$ band induced by the AFM ordering of Eu, indicating a strong interplay between the two sublattices.²⁷ Undoubtedly, detailed knowledge about the evolution of magnetic structures of both Eu and Fe with the temperature will be crucial for understanding these observations.

Isovalent substitution of Eu with Ca offers an ideal platform for studying the delicate interplay between the two magnetic sublattices. On the one hand, under ambient pressure, Ca doping into the Eu site does not perturb the SDW order in the FeAs layers visibly and never leads to SC. On the other hand, dilution of the Eu sublattice with nonmagnetic Ca^{2+} ions suppresses its AFM ordering temperature (T_{Eu}) gradually.^{38–40} A

recent μ SR study on $\text{Eu}_{0.5}\text{Ca}_{0.5}\text{Fe}_2\text{As}_2$ suggests a long-range magnetically ordered Eu sublattice.³⁹ However, it was proposed based on macroscopic measurements that substitution of 50 % Eu ions might lead to a short-range ordered nature of Eu magnetism.⁴³ In order to determine the ground-state magnetic structure of $\text{Eu}_{0.5}\text{Ca}_{0.5}\text{Fe}_2\text{As}_2$ and check the interplay between two sublattices, we have performed the temperature-dependent polarized and unpolarized neutron diffraction studies on the $\text{Eu}_{0.5}\text{Ca}_{0.5}\text{Fe}_2\text{As}_2$ single crystal. The Eu^{2+} moments are found to be long-range ordered below $T_{\text{Eu}} = 10$ K, in the A-typed AFM structure. A spin-reorientation of the Fe^{2+} moments is clearly observed around T_{Eu} , providing a direct evidence of a strong coupling between the Fe and Eu magnetism.

II. EXPERIMENTAL DETAILS

Single crystals of $\text{Eu}_{1-x}\text{Ca}_x\text{Fe}_2\text{As}_2$ ($x = 0.5$ nominally) were grown using the Sn flux method.³⁹ No incorporation of Sn into the crystals was evidenced according to the energy-dispersive x-ray spectroscopy (EDX) characterization. The concentration of Ca was determined to be 52(4) % by nuclear structure refinement of the neutron diffraction data, as presented below. A 88 mg platelike single crystal with dimensions $\sim 4 \times 3 \times 0.6$ mm³ was selected for unpolarized and polarized neutron diffraction measurements, which were performed on the hot-neutron four-circle diffractometer HEiDi and diffuse scattering cold-neutron spectrometer DNS, respectively, at Heinz Maier-Leibnitz Zentrum (MLZ), Garching (Germany).^{41,42} For measurements at both beamlines, the single-crystal sample was mounted on a thin aluminum plate with tiny amount of GE varnish and put inside a standard closed-cycle cryostat. At HEiDi, a Ge (3 1 1) monochromator was chosen to produce a monochromatic neutron beam with the wavelength of 1.17 Å, and an Er filter was used to minimize the $\lambda/2$ contamination. At DNS, the wavelength of the incident neutrons is 4.2 Å. The $[0, 1, 0]$ direction of the crystal was aligned perpendicular to the horizontal scattering plane, so that the $(H, 0, L)$ reciprocal plane can be mapped out by rotating the sample. Throughout this paper, the orthorhombic notation (space group $Fmmm$) will be used for convenience. Single crystals from the same batches were characterized by macroscopic measurements including the resistivity, heat capacity, and dc magnetic susceptibility, using a Quantum Design physical property measurement system (PPMS) and Quantum Design magnetic property measurement system (MPMS).

III. EXPERIMENTAL RESULTS

Macroscopic properties of $\text{Eu}_{0.5}\text{Ca}_{0.5}\text{Fe}_2\text{As}_2$ single crystal was shown in Fig. S1 and S2 in the Supplementary Materials. Two magnetic transitions corresponding to the SDW ordering of the Fe sublattice and AFM ordering of the Eu^{2+} moments are identified around 190 K and 10 K, respectively.

To clarify the ground-state magnetic structure of

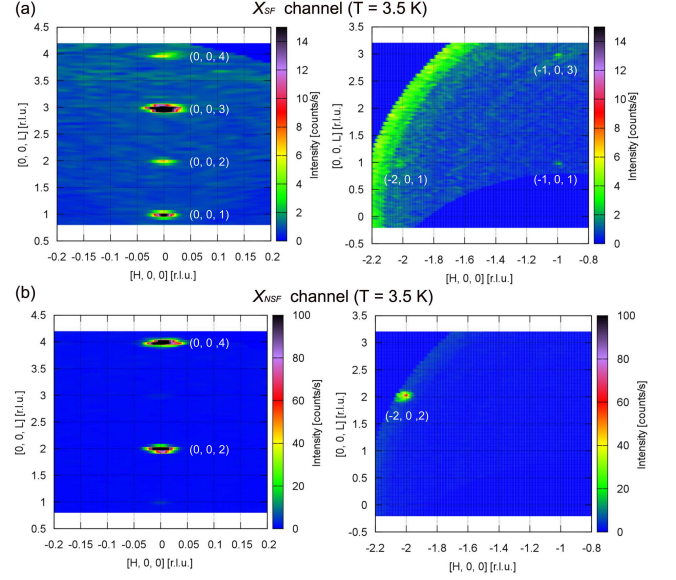


Figure 1: Reciprocal-space contour maps in the $(H, 0, L)$ plane for $\text{Eu}_{0.5}\text{Ca}_{0.5}\text{Fe}_2\text{As}_2$ obtained at $T = 3.5$ K via polarized neutron diffraction at DNS, with the neutron polarization parallel to the scattering vector Q (x polarization). Intensities in the SF (a) and NSF (b) channels correspond to the magnetic and nuclear reflections, respectively. The appearances of $(0, 0, 2)$ and $(0, 0, 4)$ reflections in the X_{SF} channel are due to the imperfection of the polarization analysis and leakage from the X_{NSF} channel.

$\text{Eu}_{0.5}\text{Ca}_{0.5}\text{Fe}_2\text{As}_2$, polarized neutron diffraction at 3.5 K was firstly performed at DNS. Fig. 1(a) and 1(b) show the reciprocal-space contour maps of the $(H, 0, L)$ plane, measured with the neutron polarization parallel to the scattering vector Q (x polarization). The magnetic and nuclear scattering were separated into the spin-flip (SF, Fig. 1(a)) and non-spin-flip (NSF, Fig. 1(b)) channels, respectively.⁴⁶ The appearance of $(0, 0, 1)$, $(0, 0, 3)$ and $(-2, 0, 1)$ reflections in the X_{SF} channel clearly indicates that the Eu^{2+} moments are antiferromagnetically ordered at 3.5 K, with a propagation vector of $k = (0, 0, 1)$, similar to the undoped parent compound EuFe_2As_2 .²⁰ Since magnetic neutron scattering is sensitive to the moment component perpendicular to Q , the Eu moments cannot be pointing along the c -axis. Due to imperfection of the polarization analysis, the strong nuclear reflections $(0, 0, 2)$ and $(0, 0, 4)$ observed in the X_{NSF} channel also leaked into the X_{SF} channel. No intensity is observed at $(-2, 0, 0)$ within the experimental resolution, excluding the possibility of a canted-AFM structure of Eu with a net ferromagnetic component along the c axis.³⁴ In addition, magnetic reflections at $(-1, 0, 1)$ and $(-1, 0, 3)$ show up in the X_{SF} channel, arising from the SDW ordering of the Fe moments with the propagation vector of $k = (1, 0, 1)$.²⁰

As shown in the inset of Fig. 2, the $(0, 0, 3)$ magnetic reflection due to the AFM ordering of Eu disappears completely at 11 K in the X_{SF} channel. The temperature dependence of its integrated intensity from the rocking scan is plotted in Fig. 2, indicating an ordering temperature of $T_{\text{Eu}} = 10.0(5)$ K, well consistent with that from the macroscopic measurements.

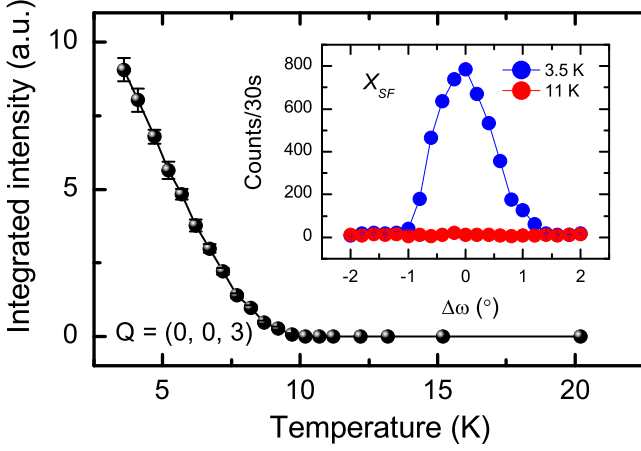


Figure 2: The temperature dependence of the integrated intensity of the (0, 0, 3) magnetic reflection in the X_{SF} channel measured at DNS. The insets show the rocking scan of the (0, 0, 3) peak at 3.5 K and 11 K, respectively.

The temperature dependence of the integrated intensity, which is proportional to the square of the order parameter, shows a very unusual behaviour. Starting with a negative curvature around T_{Eu} , it continues nearly linearly down to the lowest temperature reached in this experiment. Neither typical critical behaviour, nor tendency to saturation can be seen. As discussed below, we attribute this unusual temperature dependence to the interaction between the Eu and Fe sublattices.

The peak intensities of the (1, 0, 1) and (1, 0, 3) reflections in the X_{SF} channel, both arising from the SDW ordering of Fe, were monitored at DNS and plotted using dark spheres in Fig. 3(b) and 3(c), respectively, as a function of the temperature. The onset temperature of the SDW ordering can be estimated to be $T_{SDW} = 192(2)$ K, consistent with that the high-temperature anomaly shown in the resistivity and specific heat data. Interestingly, both order parameters display a kink at the AFM ordering temperature of Eu ($T_{Eu} = 10$ K). Below T_{Eu} , the peak intensity of (1 0 1) reflection increases steadily, while (1 0 3) weakens visibly with decreasing temperature. As shown in the insets of Fig. 3(b) and 3(c), rocking scans of the (1, 0, 1) and (1, 0, 3) reflections in the X_{SF} channel indeed show opposite temperature-dependent tendencies. The temperature dependencies of the integrated intensity of both reflections were also measured at the four-circle neutron diffractometer HEiDi. The same behaviors were observed as shown using the open circles in Fig. 3(b) and 3(c), further confirming the different responses of (1, 0, 1) and (1, 0, 3) reflections to the AFM ordering of the Eu^{2+} moments and suggesting a possible spin-reorientation of the Fe sublattice below T_{Eu} . Fig. 3(a) also shows the temperature dependencies of the integrated intensity and full width at half maximum (FWHM) of the (4, 0, 0) nuclear reflection measured at HEiDi. The sudden jump of the intensity and broadening of the peak width indicates the occurrence of a structural phase transition in $\text{Eu}_{0.5}\text{Ca}_{0.5}\text{Fe}_2\text{As}_2$ from a tetragonal (space group $I4/mmm$) to an orthorhombic (space group $Fmmm$) phase at $T_S = 191(2)$ K, coincident with the SDW ordering of Fe at

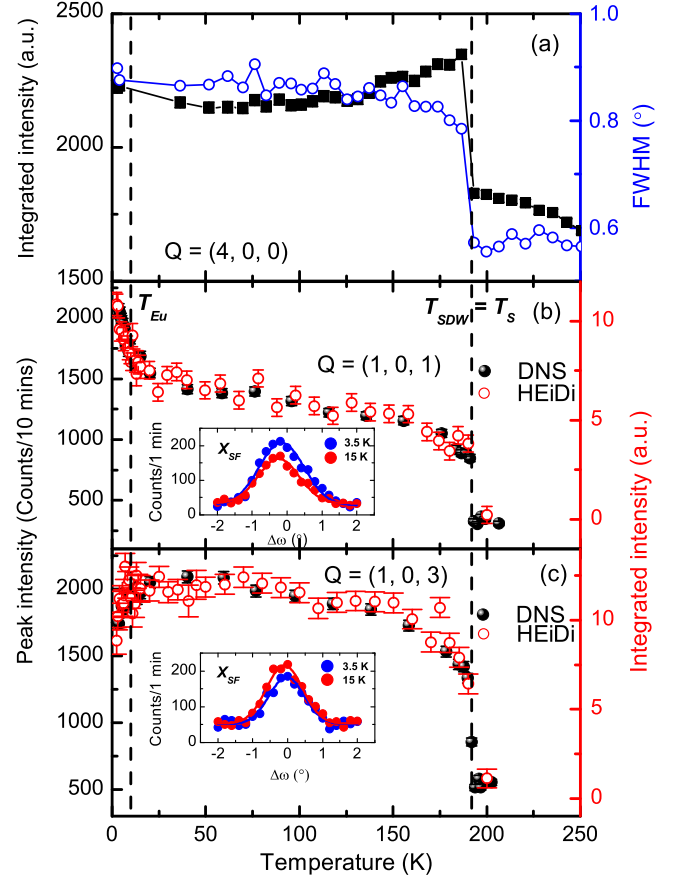


Figure 3: The temperature dependencies of the integrated intensity of the (4, 0, 0) nuclear reflection (black squares, a), (1, 0, 1) magnetic reflection (black spheres, b) and (1, 0, 3) magnetic reflection (black spheres, c), respectively, measured at HEiDi. The peak width (FWHM) of (4, 0, 0) is also plotted using blue open circles in (a). Red open circles in (b) and (c) represent the peak intensities of (1, 0, 1) and (1, 0, 3) as a function of the temperature, respectively, measured in the X_{SF} channel at DNS. The insets in (b) and (c) show the rocking scans of the (1, 0, 1) and (1, 0, 3) reflections in the X_{SF} channel at 3.5 K and 15 K, respectively. The solid curves represent the fits using the Gaussian profiles. The dashed vertical lines mark the SDW transition (T_{SDW}) coincident with the structural phase transition (T_S) and the magnetic ordering of localized Eu^{2+} moments (T_{Eu}), respectively.

T_{SDW} , due to the change of extinction conditions of strong nuclear Bragg reflections caused by the emergent orthorhombic domains.

To better understand the interplay of the magnetism between Eu and Fe sublattices in $\text{Eu}_{0.5}\text{Ca}_{0.5}\text{Fe}_2\text{As}_2$, the integrated intensities of 357 nuclear reflections and 254 magnetic reflections from Eu were collected at HEiDi at the base temperature (2.5 K). In addition, 246 nuclear reflections were collected above T_{Eu} (11 K). The obtained data sets at both temperatures were normalized to the monitor and corrected by the Lorentz factor. After the absorption correction procedure using the DATAP program taking into account the dimensions of the crystal,⁴⁷ equivalent reflections were merged into the unique ones based on the orthorhombic symmetry.

Table I: Refined results for the nuclear structure and Eu magnetic structure of $\text{Eu}_{0.5}\text{Ca}_{0.5}\text{Fe}_2\text{As}_2$ at 2.5 K, as well as the nuclear structure at 11 K. The atomic positions are as follows: Eu/Ca, $4a$ (0, 0, 0); Fe, $8f$ (0.25, 0.25, 0.25); As, $8i$ (0, 0, z). The occupancies of Eu and Ca were refined at 2.5 K and fixed at 11 K, to be 48(4)% and 52(4)%, respectively. (Space group: $Fmmm$, $a = 5.524(2)$ Å, $b = 5.521(1)$ Å, $c = 11.94(1)$ Å)

Eu/Ca	B (Å ²)	2.5 K nuclear	2.5 K Eu magnetic	11 K nuclear
	M_a (μ_B)	0.6(1)	6.74(4)	0.6(1)
Fe	B (Å ²)	0.68(4)		0.66(2)
As	z	0.3646(2)		0.3646(2)
	B (Å ²)	0.73(5)		0.70(3)
R_{F^2}		6.75	14.3	6.75
R_{wF^2}		6.14	8.49	4.51
R_F		3.60	10.9	3.57
χ^2		4.89	2.31	9.43

The nuclear structures at 2.5 K and 11 K were refined using FULLPROF.⁴⁸ As shown in Table 1, the nuclear structure does not show a visible difference below and above T_{Eu} . At 2.5 K, the magnetic reflections from Eu can be well fitted using the A-type AFM structure as confirmed for the parent compound EuFe_2As_2 ,²⁰ with the Eu^{2+} moment as large as 6.74(4) μ_B aligned along the orthorhombic a axis. Although the Eu sites are diluted with isovalent Ca^{2+} of almost 50 %, the Eu^{2+} spins are found to be long-range ordered still. This is in good agreement with a recent μSR study on the same compound,³⁹ and in stark contrast to the short-range magnetic ordering of Eu proposed for hole-doped $\text{Eu}_{0.5}\text{K}_{0.5}\text{Fe}_2\text{As}_2$ based on macroscopic measurements.⁴³

Furthermore, motivated by the intriguing responses of the magnetic order parameters of Fe in $\text{Eu}_{0.5}\text{Ca}_{0.5}\text{Fe}_2\text{As}_2$ at T_{Eu} , the integrated intensities of a few strong magnetic reflections from the Fe sublattice were collected at HEiDi by performing rocking scans, corrected by the Lorentz factor as well as the absorption effect. Fig.4 shows the integrated intensities of four magnetic reflections with relatively small statistical errors, i.e., (1, 0, 1), (1, 0, 3), (1, 2, 1) and (1, 0, 7). The intensities of them at 11 K can be very well fitted with an in-plane AFM structure of the Fe^{2+} moment (see Fig. 5(a)), with the moment size of $M_a = 1.10(5)$ μ_B along the orthorhombic a axis as calculated using FULLPROF. Both the moment direction and moment size here are quite similar to those observed for the parent compound EuFe_2As_2 in the ground state.²⁰ However, the intensities at 2.5 K clearly deviates from those predicted by the in-plane AFM structure. As neutron diffraction only probes the magnetic moment perpendicular to the scattering vector Q , the redistribution of the magnetic scattering intensities signifies a spin reorientation of the Fe^{2+} moments.⁴⁹ With a canted AFM structure which allows the Fe^{2+} moments to rotate in the ac plane (see Fig. 5(b)), the intensities at 2.5 K can be well explained with the moment size $M_a = 0.85(5)$ μ_B and $M_c = 0.22(5)$ μ_B . All the details about the model refinements of the magnetic structure of Fe were included in the Supplementary Materials.

The magnetic structures of $\text{Eu}_{0.5}\text{Ca}_{0.5}\text{Fe}_2\text{As}_2$ at 11 K and

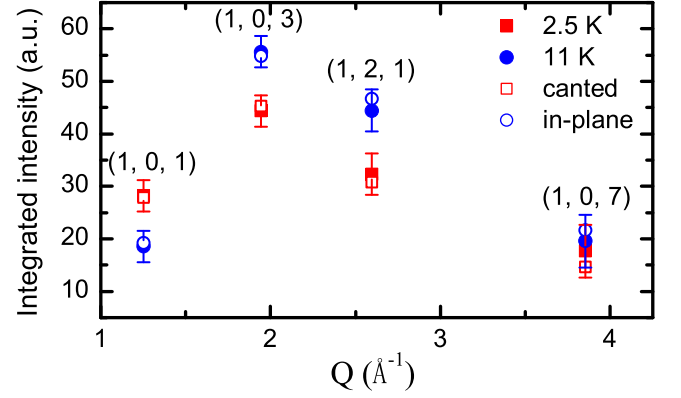


Figure 4: Comparison between the observed intensities of four magnetic reflections from the Fe sublattice at 11 K (blue filled circles), 2.5 K (red filled squares), the calculated intensities using the in-plane AFM structure (blue open circles), and the calculated intensities using the canted AFM structure (red open squares).

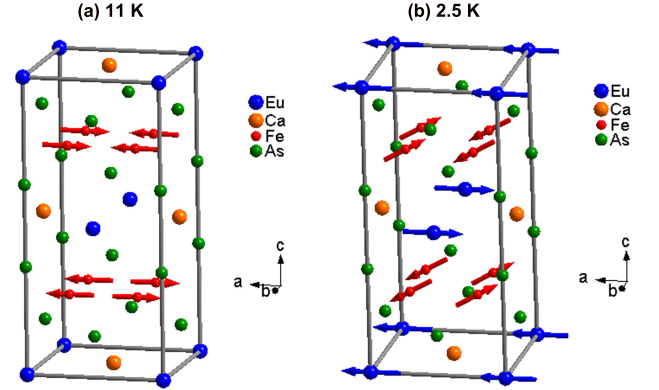


Figure 5: The magnetic structures of $\text{Eu}_{0.5}\text{Ca}_{0.5}\text{Fe}_2\text{As}_2$ at 11 K (a) and 2.5 K (b), respectively.

2.5 K are illustrated in Fig. 5(a) and 5(b), respectively. As concluded above, at 11 K (slightly above T_{Eu}), the Eu sublattice is not magnetically ordered yet while the Fe sublattice displays an in-plane AFM structure. With further decreasing temperature, the Eu^{2+} moments start to order, while the Fe^{2+} moments tend to rotate towards the c axis within the ac plane, as reflected by the opposite temperature-dependent tendencies of its magnetic order parameters shown in Fig. 3. At the reachable base temperature (2.5 K) at HEiDi, the Eu^{2+} spins are found to align along the a axis in the A-type AFM structure similar to the undoped parent compound, while the Fe^{2+} moments are ordered in a canted AFM structure with a canting angle of 14(4)° out of the ab plane. In other words, the spin reorientation of the Fe^{2+} moments occurs in coincidence with the AFM ordering of Eu, suggesting a strong interplay between the two magnetic sublattices in $\text{Eu}_{0.5}\text{Ca}_{0.5}\text{Fe}_2\text{As}_2$.

IV. DISCUSSION AND CONCLUSION

We note that the magnetic order parameter of the Eu sublattice in Fig. 2 does not saturate down to 3.5 K. However, refinements using the magnetic reflections from Eu yield the moment size of $6.74(4) \mu_B$, well consistent with a full moment of $\mu_S = gS = 7 \mu_B$ expected for the Eu^{2+} spins with $S = 7/2$. This means that the Eu sublattice is fully magnetically ordered at 3.5 K. Thus, the unusual temperature dependence in Fig. 2 is very likely to arise from the change of the strength of Eu-Fe magnetic interaction concomitant with the spin reorientation of the Fe^{2+} spins moments. As well documented, the coupling between two AFM sublattices may arise from quantum fluctuations via the so-called “order-by-disorder” mechanism.^{50–53} The strong Eu-Fe coupling in $\text{Eu}_{0.5}\text{Ca}_{0.5}\text{Fe}_2\text{As}_2$, therefore, might be due to the longitudinal fluctuations of the Eu^{2+} spins, which lead to a considerable change in the magnetic anisotropy energy and result in the spin reorientation of the Fe^{2+} moments. For the EuFe_2As_2 system, to the best of our knowledge, our observation here provides the first experimental evidence of spin reorientation of Fe below the Eu magnetic ordering temperature. $\text{Eu}_{0.5}\text{Ca}_{0.5}\text{Fe}_2\text{As}_2$, therefore, exhibits a strong Eu-Fe interplay undoubtedly. However, this is not contradictory with the weak Eu-Fe coupling in the parent compound EuFe_2As_2 ,^{20–22} since it was found that the strength of interplay between $3d$ and $4f$ electrons can be tunable by chemical doping.⁵⁴ Compared with undoped EuFe_2As_2 , the out-of-plane lattice constant c shrinks considerably by $\sim 1\%$ upon 50 % Ca substitution. As a result, the nearest Eu-Fe distance reduces by 0.7% from 3.591 Å (in EuFe_2As_2) to 3.567 Å (in

$\text{Eu}_{0.5}\text{Ca}_{0.5}\text{Fe}_2\text{As}_2$), favoring a stronger Eu-Fe spin interaction. Further theoretical studies on $\text{Eu}_{0.5}\text{Ca}_{0.5}\text{Fe}_2\text{As}_2$ will be very helpful for understanding its intriguing magnetic properties and strong Eu-Fe interplay in it.

In conclusion, using complementary polarized and unpolarized single-crystal neutron diffraction, we have investigated the temperature-dependent magnetic structures of $\text{Eu}_{0.5}\text{Ca}_{0.5}\text{Fe}_2\text{As}_2$. Upon 50 % dilution of the Eu sites with isovalent Ca^{2+} , the Eu sublattice is found to be still long-range ordered below $T_{Eu} = 10$ K, in the A-typed AFM structure. The moment size of Eu^{2+} spins is estimated to be as large as $6.74(4) \mu_B$ at 2.5 K. The Fe sublattice undergoes a SDW transition at $T_{SDW} = 192(2)$ K and displays an in-plane AFM structure above T_{Eu} . However, at 2.5 K, the Fe^{2+} moments are found to be ordered in a canted AFM structure with a canting angle of $14(4)^\circ$ out of the ab plane. The spin reorientation of Fe below the AFM ordering temperature of Eu provides a direct evidence of a strong interplay between the two magnetic sublattices in $\text{Eu}_{0.5}\text{Ca}_{0.5}\text{Fe}_2\text{As}_2$.

Acknowledgments

W. T. J. would like to acknowledge S. Mayr for the assistance with the orientation of the crystal. This work is based on experiments performed at the HEiDi and DNS instrument operated by Jülich Centre for Neutron Science (JCNS) at the Heinz Maier-Leibnitz Zentrum (MLZ), Garching, Germany. Z. B. acknowledges financial support from National Science Center, Poland Grant 2017/25/B/ST3/02868.

* Electronic address: jwt2006@gmail.com

- ¹ Y. Kamihara, T. Watanabe, M. Hirano, and H. Hosono, *J. Am. Chem. Soc.* **130**, 3296 (2008).
- ² X. H. Chen, T. Wu, G. Wu, R. H. Liu, H. Chen, and D. F. Fang, *Nature* **453**, 761 (2008).
- ³ G. F. Chen, Z. Li, D. Wu, G. Li, W. Z. Hu, J. Dong, P. Zheng, J. L. Luo, and N. L. Wang, *Phys. Rev. Lett.* **100**, 247002 (2008).
- ⁴ Z.-A. Ren, G.-C. Che, X.-L. Dong, J. Yang, W. Lu, W. Yi, X. -L. Shen, Z.-C. Li, L.-L. Sun, F. Zhou, et al., *Europhys. Lett.* **83**, 17002 (2008).
- ⁵ C. Wang, L. Li, S. Chi, Z. Zhu, Z. Ren, Y. Li, Y. Wang, X. Lin, Y. Luo, S. Jiang, et al., *Europhys. Lett.* **83**, 67006 (2008).
- ⁶ M. Rotter, M. Tegel, and D. Johrendt, *Phys. Rev. Lett.* **101**, 107006 (2008).
- ⁷ A. S. Sefat, R. Jin, M. A. McGuire, B. C. Sales, D. J. Singh, and D. Mandrus, *Phys. Rev. Lett.* **101**, 117004 (2008).
- ⁸ S. Zapf and M. Dressel, *Rep. Prog. Phys.* **80**, 016501 (2017).
- ⁹ D. C. Johnston, *Adv. Phys.* **59**, 803 (2010).
- ¹⁰ P. Dai, *Rev. Mod. Phys.* **87**, 855 (2015).
- ¹¹ D. H. Ryan, J. M. Cadogan, C. Ritter, F. Canepa, A. Palenzona, and M. Putti, *Phys. Rev. B* **80**, 220503 (2009).
- ¹² Z. Ren, Q. Tao, S. Jiang, C. Feng, C. Wang, J. Dai, G. Cao, and Z. Xu, *Phys. Rev. Lett.* **102**, 137002 (2009).
- ¹³ H. S. Jeevan, D. Kasinathan, H. Rosner, and P. Gegenwart, *Phys. Rev. B* **83**, 054511 (2011).
- ¹⁴ Z. Guguchia, A. Shengelaya, A. Maisuradze, L. Howard, Z. Bukowski, M. Chikviani, H. Luetkens, S. Katrych, J. Karpinski, and H. Keller, *J. Supercond. Nov. Magn.* **26**, 285 (2013).
- ¹⁵ H. Maeter, H. Luetkens, Y. G. Pashkevich, A. Kwadrin, R. Khasanov, A. Amato, A. A. Gusev, K. V. Lamonova, D. A. Chervinskii, R. Klingeler, et al., *Phys. Rev. B* **80**, 094524 (2009).
- ¹⁶ Q. Zhang, W. Tian, H. Li, J.-W. Kim, J. Yan, R. W. McCallum, T. A. Lograsso, J. L. Zarestky, S. L. Bud'ko, R. J. McQueeney, et al., *Phys. Rev. B* **88**, 174517 (2013).
- ¹⁷ S. Nandi, Y. Su, Y. Xiao, S. Price, X. F. Wang, X. H. Chen, J. Herrero-Martín, C. Mazzoli, H. C. Walker, L. Paolasini, et al., *Phys. Rev. B* **84**, 054419 (2011).
- ¹⁸ U. Stockert, N. Leps, L. Wang, G. Behr, S. Wurmehl, B. Büchner, and R. Klingeler, *Phys. Rev. B* **86**, 144407 (2012).
- ¹⁹ W. Tian, W. Ratcliff, M. G. Kim, J.-Q. Yan, P. A. Kienzie, Q. Huang, B. Jensen, K. W. Dennis, R. W. McCallum, T. A. Lograsso, et al., *Phys. Rev. B* **82**, 060514 (2010).
- ²⁰ Y. Xiao, Y. Su, M. Meven, R. Mittal, C. M. N. Kumar, T. Chatterji, S. Price, J. Persson, N. Kumar, S. K. Dhar, A. Thamizhavel, and Th. Brueckel, *Phys. Rev. B* **80**, 174424 (2009).
- ²¹ J. Herrero-Martín, V. Scagnoli, C. Mazzoli, Y. Su, R. Mittal, Y. Xiao, Th. Brueckel, N. Kumar, S. K. Dhar, A. Thamizhavel, and L. Paolasini, *Phys. Rev. B* **80**, 134411 (2009).
- ²² H. S. Jeevan, Z. Hossain, D. Kasinathan, H. Rosner, C. Geibel, and P. Gegenwart, *Phys. Rev. B* **78**, 052502 (2008).

- ²³ A. Pogrebna, T. Mertelj, N. Vujčić, G. Cao, Z. A. Xu, and D. Mihailovic, *Sci. Rep.* **5**, 7754 (2015).
- ²⁴ A. Ahmed, M. Itou, S. Xu, Z. Xu, G. Cao, Y. Sakurai, J. Penner-Hahn, and A. Deb, *Phys. Rev. Lett.* **105**, 207003 (2010).
- ²⁵ Z. Guguchia, J. Roos, A. Shengelaya, S. Katrych, Z. Bukowski, S. Weyeneth, F. Murányi, S. Strässle, A. Maisuradze, J. Karpinski, et al., *Phys. Rev. B* **83**, 144516 (2011).
- ²⁶ A. Błachowski, K. Ruebenbauer, J. Żukrowski, Z. Bukowski, K. Rogacki, P. J. W. Moll, and J. Karpinski, *Phys. Rev. B* **84**, 174503 (2011).
- ²⁷ W. T. Jin, Y. Xiao, Y. Su, S. Nandi, W. H. Jiao, G. Nisbet, S. Demirdis, G. H. Cao, and T. Brückel, *Phys. Rev. B* **93**, 024517 (2016).
- ²⁸ Y. Xiao, Y. Su, W. Schmidt, K. Schmalzl, C. M. N. Kumar, S. Price, T. Chatterji, R. Mittal, L. J. Chang, S. Nandi, et al., *Phys. Rev. B (R)* **81**, 220406 (2010).
- ²⁹ Y. Xiao, Y. Su, S. Nandi, S. Price, B. Schmitz, C. M. N. Kumar, R. Mittal, T. Chatterji, N. Kumar, S. K. Dhar, et al., *Phys. Rev. B* **85**, 094504 (2012).
- ³⁰ W. T. Jin, S. Nandi, Y. Xiao, Y. Su, O. Zaharko, Z. Guguchia, Z. Bukowski, S. Price, W. H. Jiao, G. H. Cao, and Th. Brückel, *Phys. Rev. B* **88**, 214516 (2013).
- ³¹ S. Nandi, W. T. Jin, Y. Xiao, Y. Su, S. Price, D. K. Shukla, J. Strempfer, H. S. Jeevan, P. Gegenwart, and Th. Brückel, *Phys. Rev. B* **89**, 014512 (2014).
- ³² S. Nandi, W. T. Jin, Y. Xiao, Y. Su, S. Price, W. Schmidt, K. Schmalzl, T. Chatterji, H. S. Jeevan, P. Gegenwart, and Th. Brückel, *Phys. Rev. B* **90**, 094407 (2014).
- ³³ W. T. Jin, W. Li, Y. Su, S. Nandi, Y. Xiao, W. H. Jiao, M. Meven, A. P. Sazonov, E. Feng, Y. Chen, C. S. Ting, G. H. Cao, and Th. Brückel, *Phys. Rev. B* **91**, 064506 (2015).
- ³⁴ W. T. Jin, Y. Xiao, Z. Bukowski, Y. Su, S. Nandi, A. P. Sazonov, M. Meven, O. Zaharko, S. Demirdis, K. Nemkovski, et al., *Phys. Rev. B* **94**, 184513 (2016).
- ³⁵ W. T. Jin, J. P. Sun, G. Z. Ye, Y. Xiao, Y. Su, K. Schmalzl, S. Nandi, Z. Bukowski, Z. Guguchia, E. Feng, et al., *Sci. Rep.* **7**, 3532 (2017).
- ³⁶ R. Marchand and W. Jeitschko, *J. Solid State Chem.* **24**, 351 (1978).
- ³⁷ S. Jiang, H. Xing, G. Xuan, Z. Ren, C. Wang, Z. A. Xu, and G. Cao, *Phys. Rev. B* **80**, 184514 (2009).
- ³⁸ A. Mitsuda, S. Seike, T. Matoba, H. Wada, F. Ishikawa, and Y. Yamada, *J. Phys. Conf. Ser.* **273**, 012100 (2011).
- ³⁹ L. M. Tran, M. Babij, L. Korosec, T. Shang, Z. Bukowski, and T. Shiroka, *Phys. Rev. B* **98**, 104412 (2018).
- ⁴⁰ L. Harnagea, R. Kumar, S. Singh, S. Wurmehl, A. U. B. Wolter, and B. Büchner, *J. Phys. Condens. Matter* **30**, 415601 (2018).
- ⁴¹ M. Meven and A. Sazonov, *J. Large-Scale Res. Facilities* **1**, A7 (2015), URL <http://dx.doi.org/10.17815/jlsrf-1-20>.
- ⁴² Y. Su, K. Nemkovski, and S. Demirdis, *J. Large-Scale Res. Facilities* **1**, A27 (2015), URL <http://dx.doi.org/10.17815/jlsrf-1-33>.
- ⁴³ H. S. Jeevan, Z. Hossain, D. Kasinathan, H. Rosner, C. Geibel, and P. Gegenwart, *Phys. Rev. B* **78**, 092406 (2008).
- ⁴⁴ W. T. Jin, N. Qureshi, Z. Bukowski, Y. Xiao, S. Nandi, M. Babij, Z. Fu, Y. Su, and T. Brückel, *Phys. Rev. B* **99**, 014425 (2019).
- ⁴⁵ K. Komadera, A. Błachowski, K. Ruebenbauer, J. Żukrowski, S. M. Dubiel, L. M. Tran, B. M., and Z. Bukowski, *J. Magn. Magn. Mater.* **457**, 1 (2018).
- ⁴⁶ O. Schärpf and H. Capellmann, *Phys. Stat. Sol. A* **135**, 359 (1993).
- ⁴⁷ P. Coppens, L. Leiserowitz, and D. Rabinovich, *Acta Crystallogr.* **18**, 1035 (1965).
- ⁴⁸ J. Rodríguez-Carvajal, *Physica B* **192**, 55 (1993).
- ⁴⁹ F. Waßer, A. Schneidewind, Y. Sidis, S. Wurmehl, S. Aswartham, B. Büchner, and M. Braden, *Phys. Rev. B* **91**, 060505 (2015).
- ⁵⁰ T. Brueckel, B. Dorner, A. G. Gukasov, V. P. Plakhty, W. Prandl, E. F. Shender, and O. P. Smirnow, *Z. Phys. B* **72**, 477 (1988).
- ⁵¹ T. Brückel, B. Dorner, A. Gukasov, and V. Plakhty, *Phys. Lett. A* **162**, 357 (1992).
- ⁵² T. Brueckel, C. Paulsen, K. Hinrichs, and W. Prandl, *Z. Phys. B* **97**, 391 (1995).
- ⁵³ A. G. Gukasov, T. Brückel, B. Dorner, V. P. Plakhty, W. Prandl, E. F. Shender, and O. P. Smirnov, *Europhys. Lett.* **7**, 83 (1988).
- ⁵⁴ T. Shang, L. Yang, Y. Chen, N. Cornell, F. Ronning, J. L. Zhang, L. Jiao, Y. H. Chen, J. Chen, A. Howard, et al., *Phys. Rev. B* **87**, 075148 (2013).